8. Astrophysical Examples of Line Processes

8.1 Spectra of Gaseous Nebulae

References:

- R. E. Williams, *Gaseous Nebulae*
- D. E. Osterbrock, *Astrophysics of Gaseous Nebulae*

Refer to page **??** for some examples of planetary nebulae spectra; these are representative of gaseous nebulae in general except that the emission tends to be stronger due to higher densities. But the radiation mechanisms responsible for the continua, the permitted lines, and the forbidden lines are common to all nebulae.

The optical continuum from gaseous nebulae is produced by recombination and the radio continuum by thermal bremsstrahlung. Here, we shall concern ourselves with line emission only; that is, bound-bound transitions. In this connection, there are two mechanisms for populating the excited states: (i) recombination which is responsible for the permitted emission lines observed in nebulae, and (ii) collisional excitation which is responsible for the forbidden lines which can be *even stronger* than the permitted ones!

(a) Hydrogen Recombination Lines

The line flux in the *optically thin* case is simply

$$F_\nu = \frac{1}{D^2}\int_0^R \epsilon_\nu(r)\, r^2\, dr$$

for a spherical geometry. The emissivity ϵ_ν is related to the emission coefficient j_ν by

$$\epsilon_\nu = 4\pi j_\nu = 4\pi j_{nn'} = N_n A_{nn'}\, h\nu_{nn'} \ .$$

To compute the population numbers N_n, it is common to assume *statistical equilibrium*; that is, a steady state condition. In the case of nebulae, we are dealing with a *dilute* gas (low density and weak radiation field). In such environments, all the relevant states for permitted transitions are populated only by *recombinations* (directly or indirectly by cascades from higher states) and depopulated by *spontaneous de-excitations*. An exception to this rule arises from the fact that most nebulae are optically thick to Lyman line radiation. In this case, upper states can also be populated by radiative transitions from the ground state.

Population rate for level n:

$$\mathcal{P}_n = N_e N_i\, \langle \sigma_n^{(\mathrm{rec})} v\rangle + \sum_{n'=n+1}^{\infty} N_{n'} A_{n'n} \ .$$

Depopulation rate for level n:

$$\mathcal{D}_n = N_n \sum_{n'=1,2}^{n-1} A_{nn'} \ .$$

Whether the lower limit here on n' is 1 or 2 depends on whether the nebula is optically thin in the Lyman lines (Menzel Case A) or optically thick (Menzel Case B). The reason for the difference is that a transition to $n' = 1$ produces a Lyman line photon which is immediately absorbed back to state n again IF Case A applies. Thus, under optically thick conditions, every transition to $n' = 1$ is balanced by its inverse, resulting in no net depopulation via this route. Therefore, we can subtract these processes off both sides of the statistical equilibrium equation. This is the normal situation which we will assume here for the remainder of this argument. The expression for $\mathcal{P}_n$ already incorporates this assumption by ignoring radiative excitations from the ground state.

The "capture-cascade" equation (statistical equilibrium) then becomes $\mathcal{P}_n = \mathcal{D}_n$ or

$$N_e N_i \, \langle \sigma_n^{(\mathrm{rec})} v \rangle + \sum_{n'=n+1}^{\infty} N_{n'} A_{n'n} = N_n \sum_{n'=2}^{n-1} A_{nn'} \; .$$

We see that there is one equation for each level n and, hence, an *infinite* number! For this problem, however, we can make a simplifying approximation: consider a *finite* number of levels corresponding to some *maximum* level m. The rationale behind this is that the influence of the very high states is *small* because the recombination probability is *low* for high n as pointed out earlier in these notes. From Osterbrock's book (p16-17) and p120 of these notes, we have

$$\langle \sigma_n^{(\mathrm{rec})} v \rangle \propto \frac{1}{n \, T_e^{1/2}}$$

which is the total, integrated over all velocities. In magnitude, $\sigma_n^{(\mathrm{rec})} \sim 10^{-21} - 10^{-20}\,\mathrm{cm}^2$ which is much smaller than the actual physical atomic cross-section of a neutral atom ($\sim 10^{-16}\,\mathrm{cm}^2$) but much larger than the physical cross-section of the nucleus ($\sim 10^{-26}\,\mathrm{cm}^2$).

Remember that the cross-section as a function of velocity, $\sigma_n^{\mathrm{rec}}(v)$, is proportional to n^{-3} just like the photoionization coefficient $\alpha_{n\nu}$ that we derived earlier. But averaging over v reduces the dependence to n^{-1}. The same thing would happen to $\alpha_{n\nu}$ if we averaged it over all $h\nu > \chi_n$.

We begin the reduction with this somewhat arbitrary maximum level m. Since there are no relevant levels with $n' > m$ (by assumption), we can write

$$N_e N_i \, \langle \sigma_m^{(\mathrm{rec})} v \rangle = N_m \sum_{n'=2}^{m-1} A_{mn'} \qquad (n = m) \, .$$

Solving for N_m, we find

$$N_m = N_e N_i \, \frac{\langle \sigma_m^{(\mathrm{rec})} v \rangle}{S_m} = N_e N_i \, f_m(T_e)$$

where

$$S_m \equiv \sum_{n'=2}^{m-1} A_{mn'}, \qquad \text{and} \qquad f_m(T_e) \equiv \frac{\langle \sigma_m^{(\mathrm{rec})} v \rangle}{S_m} \propto \frac{1}{m \, T_e^{1/2}} \; .$$

Clearly, N_m is proportional to the recombination rate which is not surprising.

Now proceed to level $m - 1$:

$$N_e N_i \, \langle \sigma_{m-1}^{(\mathrm{rec})} v \rangle + N_m A_{m\,m-1} = N_{m-1} S_{m-1}$$

from which we derive

$$N_{m-1} = \frac{1}{S_{m-1}} [N_e N_i \, \langle \sigma_{m-1}^{(\mathrm{rec})} v \rangle + N_e N_i \, f_m(T_e) A_{m\,m-1}] = N_e N_i \, f_{m-1}(T_e)$$

where

$$f_{m-1}(T_e) = \frac{\langle \sigma^{(\mathrm{rec})}_{m-1} v \rangle S_m + \langle \sigma^{(\mathrm{rec})}_{m} v \rangle A_{m\,m-1}}{S_{m-1}} \propto \frac{1}{T_e^{1/2}} \; .$$

This procedure can be continued on down to obtain all the level populations; they look like

$$N_n = N_e N_i \, f_n(T_e) \quad \text{where} \quad f_n(T_e) \propto T_e^{-1/2} \; .$$

Note that $f_m \propto m^{-1}$ as shown on the preceding page but in general f_n $(n < m)$ will fall off more slowly than n^{-1} because it involves a sum over higher states.

Note that in general the equations of statistical equilibrium cannot be solved in such a simple fashion. Normally, there would be collisions and radiative transitions from lower levels in which case all the populations would have to be solved *simultaneously.* In addition, the radiation intensity J_ν would be needed for the radiative rates and this could involve solving the equation of radiative transfer. Another way of saying this is that, in general, the matrix whose elements are the coefficients which couple all states with one another would be *full.* But our approximation here couples states only to those higher up. This transforms the matrix into *upper diagonal form* which can be solved directly.

The Balmer Decrement

The "decrement" is the Balmer line intensity relative to the H_β line intensity; in the optically thin limit, this quantity becomes

$$D_n \equiv \frac{F_{n2}}{F_{42}} = \frac{j_{n2}}{j_{42}} = \frac{N_n \, A_{n2} \, \nu_{n2}}{N_4 \, A_{42} \, \nu_{42}} \qquad (n > 2) \, .$$

The interesting feature of this line ratio is that it is almost independent of density and temperature and effectively a function only of n. This is because both N_n and N_4 are proportional to $N_i N_e$ and all the f_n have roughly the same dependence on T_e; thus,

$$D_n = \frac{f_n(T_e) \, A_{n2} \, \nu_{n2}}{f_4(T_e) \, A_{42} \, \nu_{42}} \simeq F(n) \; .$$

The lack of any dependence on T_e is not strictly correct because the temperature dependence shown for $\langle \sigma^{(\mathrm{rec})}_n v \rangle$ on the preceding page is only approximate. Nevertheless, D_n is fairly independent of the physical conditions as you can see by looking in Osterbrock's book (near page 65) where D_n is tabulated for n up to 20. To a rough approximation, $D_n \propto n^{-3}$, reflecting the fall-off in both f_n and A_{n2} with increasing n. (Remember that $A_{n0} \propto n^{-3}$ at least for large n.) The following table shows some theoretical intensities for the lower-order Balmer lines. I believe that collisional transitions have been incorporated in some limited way because the H_α decrement is slightly density dependent.

Balmer Decrement

T_e (°K)	10^4		2×10^4	
N_e (cm^{-3})	10^2	10^6	10^2	10^6
H_α	286	281	274	272
H_β	100	100	100	100
H_γ	47	47	48	48
H_δ	26	26	26	27
H_ϵ	16	16	16	16

The absolute flux of any of these lines can be found once H_β is specified or calculated by integrating its emission coefficient over the volume of the nebula (see the expression for F_ν on the first page of this section). Note that all this analysis assumes that the Balmer lines are *optically thin* which is almost always the case because the large majority of the hydrogen atoms are in the ground state.

Examine the data on page **??**. The first table shows theoretical line intensities (based on three different models for the Lyman line radiation) compared with the mean decrement for a selection of high density nebulae. Collisional transitions have been included. The optically thick model (B) is obviously the best and we can conclude that planetary nebulae are optically thick in the Lyman lines.

The second table shows a comparison between theory and observation for the relatively low-density NGC 7662. It is somewhere between optically thin and optically thick. Collisions have been included only for high orders ($n > 20$). The theoretical intensities are not too bad at low order, but one can see systematic differences at high order. Collisions help but they don't seem to be enough.

BALMER DECREMENT IN PLANETARY NEBULAE

A. Collisional Transitions Included For All n

THE BALMER DECREMENT

λ	Observed Intensity	Theoretical Intensity		
		A	B	C
4861	10.00	10.00	10.00	10.00
4340	5.58	5.76	5.10	3.47
4101	3.13	3.74	3.10	1.62
3969	2.03	2.55	2.06	0.89
3889	1.42	1.82	1.43	0.55
3835	0.98	1.36	1.05	0.36
3797	0.75	1.05	0.79	0.25
3770	0.54	0.81	0.59	0.18
3750	0.43	0.65	0.46	0.14

Col. 2: mean intensity from 41 nebulae relative to H_β (corrected for space absorption)

Col. 3: optically thin case (A) (no Lyman line radiation from star)

Col. 4: optically thick case (B)

Col. 5: optically thin case (C) (Lyman line radiation from star)

B. Collisions Included Only For High n

COMPARISON OF OBSERVED AND PREDICTED BALMER DECREMENT FOR NGC 7662

n	I_0	I_i	I_{Rad}	I_{Int}	n	I_0	I_i	I_{Rad}	I_{Int}
3	330	279	285	285	18	1.7	2.0	0.95	1.13
4	100	100	100	100	19	1.6	1.8	.81	1.00
5	43	46	47	47	20	1.4	1.5	.70	0.90
6	19.3	21	26	26	21	1.1	1.3	.60	0.80
7	14.7	17	16	16	22	1.1	1.3	.52	0.73
8	(14.7)	(17)	11	11	23	0.86	1.0	.46	0.66
9	7.0	8.1	7.6	7.6	24	0.79	0.91	.40	0.61
10	5.9	6.8	5.5	5.6	25	0.67	0.78	.36	0.56
11	4.8	5.5	4.1	4.2	26	0.73	0.83	.32	0.51
12	4.0	4.6	3.6	3.7	27	0.63	0.72	.28	0.47
13	3.6	4.1	2.6	2.6	28	0.61	0.71	.26	0.44
14	3.7	4.2	2.0	2.1	29	0.67	0.78	.23	0.40
15	2.5	2.8	1.6	1.8	30	0.53	0.60	.21	0.38
16	2.2	2.5	1.4	1.55	31	0.49	0.56	0.19	0.35
17	2.0	2.2	1.1	1.30					

I_0 = Observed line intensity (Aller, Kaler, and Bowen 1966).
I_i = Observed intensity corrected for space absorption.
I_{Rad} = Predicted intensity for pure radiative processes to $n = 60$.
I_{Int} = Interpolated theoretical intensities to allow for gradual onset of collisional redistribution at n near 20.

PLANETARY NEBULA SPECTRA

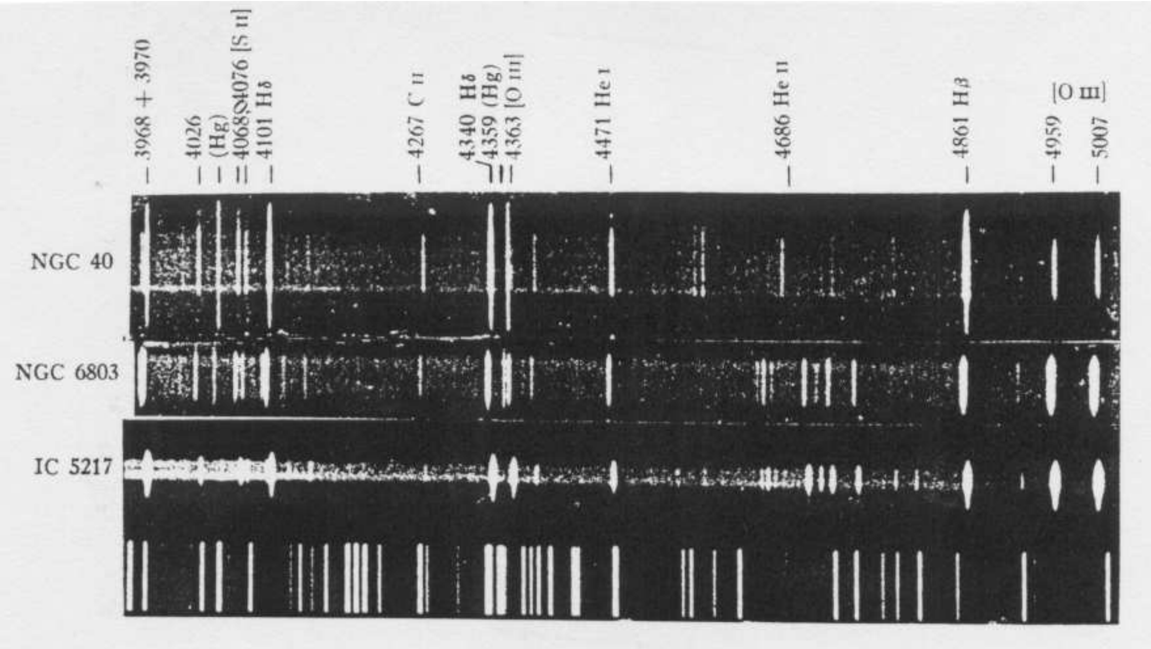

Figure 8.11 – Spectra of three planetary nebulae in the blue-violet region. One can compare the low-excitation nebula NGC 40 with objects of medium and moderately high excitation: NGC 6803 and IC 5217. (From L. H. Aller & W. Liller 1968, *Nebulae and Interstellar Matter*, eds. B. M. Middlehurst & L. H. Aller, University of Chicago Press.)

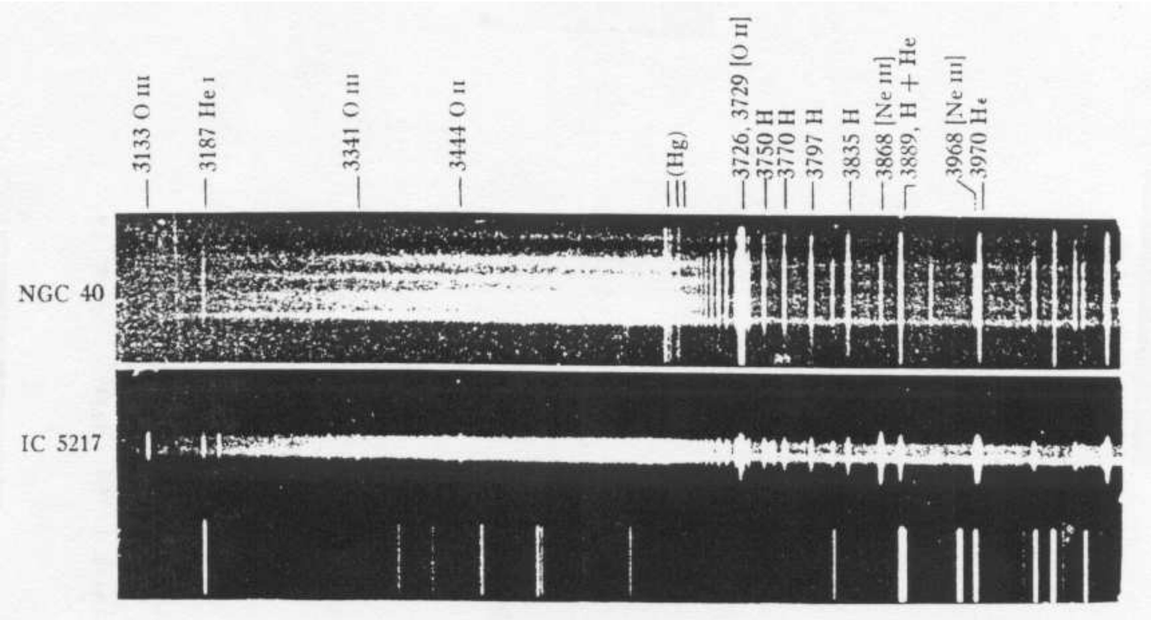

Figure 8.12 – Spectra of two planetaries in the near ultraviolet. Compare the low-excitation nebula NGC 40 with the moderately high-excitation one IC 5217. Note the paucity and weakness of lines in the ultraviolet of NGC 40 where only λ3187 He I is prominent along with the Balmer continuum. (From L. H. Aller & W. Liller 1968.)

(b) Forbidden Lines

These arise from collisional excitations from the ground state to a nearby level belonging to the same (ground) electron configuration. Thus, $\Delta\ell = 0$ and, therefore, the radiative de-excitation is *forbidden*.

The excited levels can lie only a few ev (at most) above the ground state if $T_e \sim 10^4\,°\mathrm{K}$ because this temperature corresponds to a mean particle energy of only about 1 ev. This is obviously not an option for light atoms such as H and He but it *is* for heavier elements such as O, C, and N. As we saw earlier, these radiative transitions give rise to *electric quadrapole* radiation; i.e., there is no change in the electric dipole moment of the atom or ion because $\Delta\ell = 0$.

For comparison, states responsible for permitted lines lie far above the ground state because different ℓ values are involved. Thus, permitted transitions are triggered by *recombinations* and *not* excitations.

The excitation cross-section looks like

$$\begin{aligned}\langle \sigma^{(\mathrm{exc})} v\rangle &= \int_{v_o}^{\infty} \sigma(v)\, v\, N(v)\, dv \\ &\propto \int_{v_o}^{\infty} v^{-2}\, v\, \frac{v^2}{T_e^{3/2}}\, \mathrm{e}^{-mv^2/2kT_e}\, dv \\ &\propto \frac{1}{T_e^{1/2}}\, \mathrm{e}^{-(E_n - E_o)/kT_e}\end{aligned}$$

where the threshold velocity v_o satisfies $\frac{1}{2}mv_o^2 = E_n - E_o$. Note that $\langle\sigma^{(\mathrm{exc})}\rangle$ is much larger than $\langle\sigma^{(\mathrm{rec})}\rangle$; namely, $10^{-16}\,\mathrm{cm}^2$ versus $10^{-20}\,\mathrm{cm}^2$ if $T_e \sim 10^4\,°\mathrm{K}$. Also, I have used the fact that $\sigma(v) \propto v^{-2}$ $(v > v_o)$ as shown in S. J. Czyzak, Chapter 8 in *Nebulae & Interstellar Matter*, Vol. VII, Stars & Stellar Systems.

To analyze the forbidden line problem, we consider a 2-level atom which is reasonable if the lower state is the ground and no other levels are nearby to the excited state. Excitations are generally by *electron* impact rather than by collisions with ions because the lighter particles are moving faster. Statistical equilibrium yields

$$N_e N_1 \langle \sigma_{12}\, v\rangle = N_2\,(A_{21} + N_e\langle\sigma_{21}\, v\rangle)$$

or

$$N_2 = N_e N_1 \frac{\langle\sigma_{12}\, v\rangle}{A_{21} + N_e\langle\sigma_{21}\, v\rangle}$$

and, therefore, the forbidden emission will be

$$j_{21} = N_2 A_{21} \frac{h\nu_{21}}{4\pi} = N_e N_1 \frac{h\nu_{21}}{4\pi}\left(\frac{A_{21}\langle\sigma_{12}\, v\rangle}{A_{21} + N_e\langle\sigma_{21}\, v\rangle}\right) .$$

Note that $\langle\sigma_{12}\, v\rangle$ and $\langle\sigma_{21}\, v\rangle$ are related by the principle of detailed balance:

$$\langle\sigma_{12}\, v\rangle = \langle\sigma_{21}\, v\rangle \frac{g_2}{g_1}\, \mathrm{e}^{-(E_2 - E_1)/kT_e} .$$

Now consider the equation for j_{21}. It is clear that there are two distinct regimes in density – one for low N_e and the other for high N_e. The critical electron density,

$$N_{ec} = \frac{A_{21}}{\langle\sigma_{21}\, v\rangle} \simeq N_c ,$$

is the boundary between the two. Above this density, collisional processes dominate over radiative ones. Below N_c, the spontaneous de-excitation rate is equivalent to the upward collisional rate. This boundary has a profound influence on the use of these lines for measuring density as you will see later. Typically,

$$\begin{aligned} A_{21} &\sim 10^{-4} - 1\,\mathrm{s}^{-1} \quad (\text{forbidden})\,, \\ \langle \sigma_{21} \rangle &\sim 10^{-16}\,\mathrm{cm}^2 \quad (\mathrm{T_e} \simeq 10^4\,^\circ\mathrm{K})\,, \\ \langle v_e \rangle &\sim 10^{8}\,\mathrm{cm\,s}^{-1} \quad (\mathrm{T_e} \simeq 10^4\,^\circ\mathrm{K})\,. \end{aligned}$$

Thus, N_c is typically $10^4 - 10^8\,\mathrm{cm}^{-3}$ for forbidden transitions. Obviously, the higher densities are not realized in nebulae but the lower ones can be in compact H II regions and planetary nebulae. Note, however, that laboratory densities are always higher than N_c which means that forbidden line intensities grow like N whereas recombination grows like N^2. This explains why recombination always over-powers forbidden line emission in the lab, making the latter almost impossible to observe in terrestrial situations.

In the *low density* limit,

$$j_{21} = N_e N_1 \langle \sigma_{12}\, v \rangle \frac{h\nu_{21}}{4\pi} \propto N_1^2 \text{ or } N_e^2$$

whereas, at the other extreme,

$$j_{21} = N_1 A_{21} \frac{\langle \sigma_{12}\, v \rangle}{\langle \sigma_{21}\, v \rangle} \frac{h\nu_{21}}{4\pi} \propto N_1 \text{ or } N_e\ .$$

The corresponding population levels are

$\underline{N_e \ll N_c}$:

$$\frac{N_2}{N_1} = N_e \frac{\langle \sigma_{12}\, v \rangle}{A_{21}} \quad (\text{subthermal: } T_{\mathrm{ex}} < T_e)\ ,$$

$\underline{N_e \gg N_c}$:

$$\frac{N_2}{N_1} = \frac{\langle \sigma_{12}\, v \rangle}{\langle \sigma_{21}\, v \rangle} = \frac{g_2}{g_1}\,\mathrm{e}^{-(E_2 - E_1)/kT_e} \quad (\text{thermal: } T_{\mathrm{ex}} = T_e)\ .$$

Note that at low densities, the emission grows like the *square* of the density (N_e^2) whereas, for $N_e > N_c$, the growth rate is *linear* with density. Therefore, in a $\log j - \log N_e$ plot, the slope changes from +2 to +1 as N_e passes above N_c.

It is interesting to compare the intensities of two lines whose only difference is their respective values of A_{21}. Will the high A transition give rise to a stronger line or a weaker one? The answer to this question depends on whether the critical densities fall below or above the densities at which the lines become optically thick.

For *optical* lines, A_{21} tends to be low ($\sim 10^{-4}\,\mathrm{s}^{-1}$) which corresponds to a relatively low N_c. The situation is represented in a schematic fashion in the first of the following two sketches:

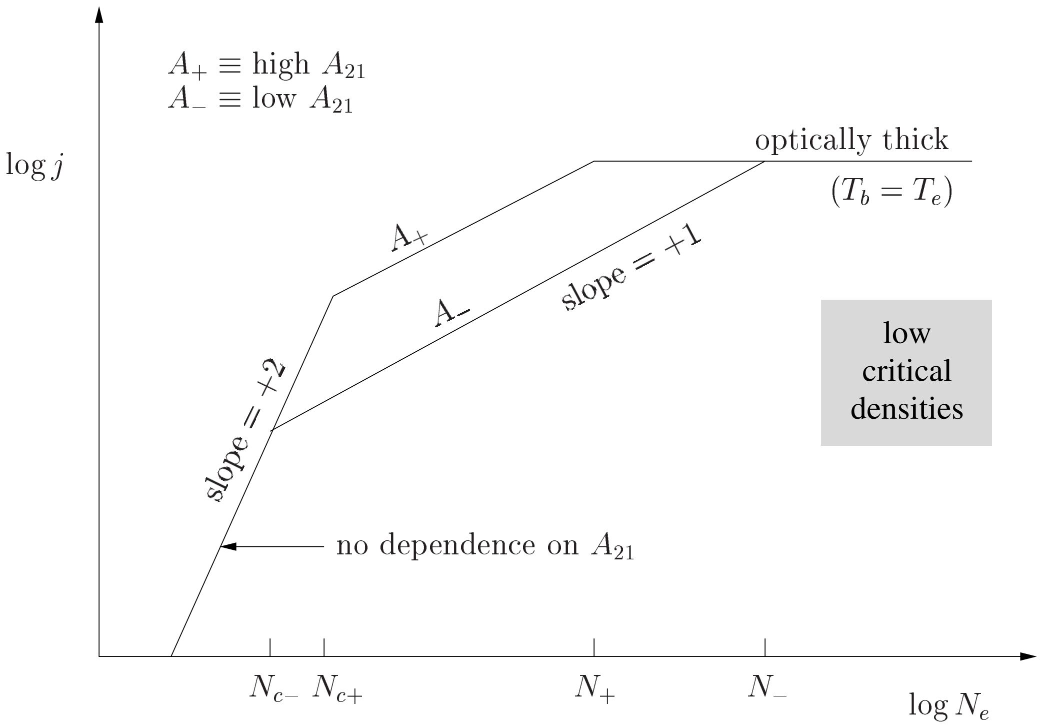

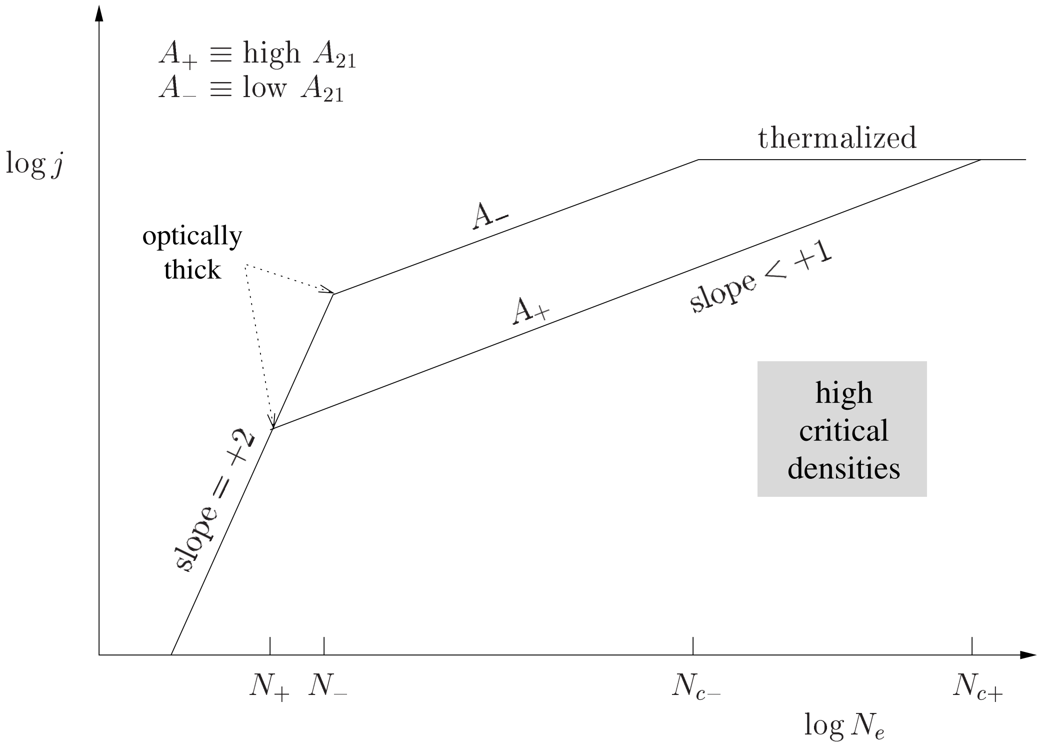

Note that the higher A_{21} transition has a higher N_c and, therefore, the intensity can grow to a higher value before the slope drops to the lower value (namely, +1). Moreover, the density (N_+) at which the high-A line becomes optically thick is *lower* than the corresponding density (N_-) for the low-A transition. This is because a high A_{21} corresponds to a high B_{12}; i.e., a high absorption coefficient. Note also that the *ratio* of line intensities is density-dependent only in the narrow range between the critical densities (see the later demonstration of this starting on page **??**).

Now, if we shift to longer wavelengths, and sources can be optically thick at densities *below* N_c. Good examples of this case are *molecular lines* at mm wavelengths; this is illustrated in the second sketch. Now you can see that the *low-A* line is *stronger* at intermediate densities. Note that above the optically thick densities (N_+ and N_-), the slope drops *below* +1. Only when the gas becomes collisionally dominated ($N_e > N_c$) do we reach the thermalized (Boltzmann) state. The above plot explains why some lines with high A are not visible at low densities whereas ones with lower A are.

Determination of Physical Parameters from Forbidden Lines

Earlier, we learned that it is difficult to get much information about temperature and density from the Balmer lines. Forbidden lines, on the other hand, can be very sensitive to T_e and N_e in particular density and temperature regimes. To see this, consider the following:

Electron Temperature

The principle involved here is to compare the line intensities from two excited states, each populated by collisions from the ground state. Because the two excited states have different energies, the degrees of collisional excitation (and, hence, line strengths originating from the two states) are sensitive to the kinetic temperature.

As an example, consider O III which has the electron configuration $1s^2\, 2s^2\, 2p^2$ and the same energy level diagram that we saw earlier for silicon:

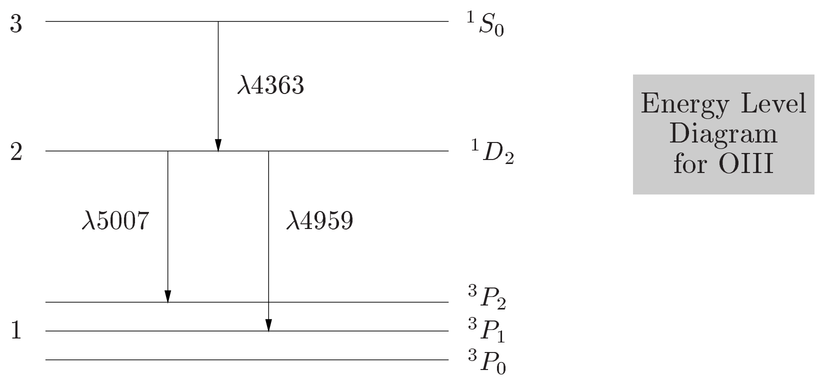

In this simplified analysis, we lump the two $2 \rightarrow 1$ transitions into *one* line (call it $\lambda 5007$). Despite being *optical* lines, both upper states have large A (A_{32} and A_{21} are both greater than $1\,\mathrm{s}^{-1}$ with A_{31} much smaller) and, thus, have critical densities above $10^8\,\mathrm{cm}^{-3}$ and certainly well above typical nebular values. This means that we can ignore all collisional transitions except those from the ground state.

In this case, statistical equilibrium imposes two conditions:

(i) the radiative rate from $3 \rightarrow 2$ must be balanced by the collision rate from $1 \rightarrow 3$, and

(ii) the radiative rate from $2 \rightarrow 1$ must be balanced by the sum of the collision rates from $1 \rightarrow 2$ and $1 \rightarrow 3$.

Thus,

$$j(\lambda 4363) = N_e N_1 \langle \sigma_{13}\, v \rangle \, \frac{h\nu_{32}}{4\pi} \,,$$

and

$$j(\lambda 5007) = N_e N_1 (\langle \sigma_{12}\, v \rangle + \langle \sigma_{13}\, v \rangle) \, \frac{h\nu_{21}}{4\pi} \,.$$

We can now evaluate the intensity ratio; note that the density cancels out:

$$\frac{j(\lambda 5007)}{j(\lambda 4363)} = \frac{\lambda_{32}}{\lambda_{21}} \left(1 + \frac{\langle \sigma_{12}\, v \rangle}{\langle \sigma_{13}\, v \rangle} \right) \,.$$

Both collision rates go like

$$\frac{g_n}{T_e^{1/2}} \, \mathrm{e}^{-(E_n - E_1)/kT_e} \,.$$

Therefore,

$$r \equiv \frac{j(\lambda 5007)}{j(\lambda 4363)} = \frac{\lambda_{32}}{\lambda_{21}} \left(1 + C \, \frac{g_2}{g_3} \, \mathrm{e}^{(E_3 - E_2)/kT_e} \right)$$

where the constant C is about 2 and the ratio of the statistical weights is 5. Allowing for the ratio of wavelengths, we can write

$$r \simeq 8 \, \mathrm{e}^{33000/T_e}$$

which is definitely sensitive to the temperature!

Electron Density

Here, we use two transitions with critical densities which *bracket* the unknown density. Obviously, some experimentation is required in choosing an appropriate line ratio. In any case, in the density range between the two N_c, the ratio of the intensities does depend on N_e as we saw earlier. Moreover, if the lines result from the *same* upper level, the intensity ratio will depend *only* on the density.

A well studied example is O II (*singly* ionized oxygen) with the electron configuration $1s^2\, 2s^2\, 2p^3$. Check back in §7.1 (p106) for the term structure; the energy level diagram looks like this if we ignore the higher doublet P-states:

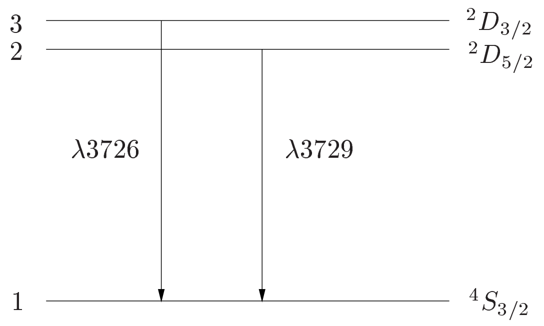

Energy Level Diagram for OII

Note the *inverted* doublet D-states due to the p-shell being half-full.

The critical densities are evaluated from

$$\begin{aligned} A_{21}(\lambda 3729) &= 4 \times 10^{-5}\,\mathrm{s}^{-1} \,, \\ A_{31}(\lambda 3726) &= 2 \times 10^{-4}\,\mathrm{s}^{-1} \,, \\ \langle \sigma_{12} \rangle, \langle \sigma_{13} \rangle &\simeq 10^{-16}\,\mathrm{cm}^2 \qquad (T_e \sim 10^4\,{}^\circ\mathrm{K}) \,. \end{aligned}$$

With this data, we obtain

$$N_c(\lambda 3729) = 4\times 10^3\,\mathrm{cm}^{-3} \quad \text{and} \quad \mathrm{N_c}(\lambda 3726) = 2\times 10^4\,\mathrm{cm}^{-3}\ .$$

In the *low density limit* ($N_e \leq 4\times 10^3\,\mathrm{cm}^{-3}$),

$$r = \frac{j(\lambda 3729)}{j(\lambda 3726)} = \frac{\langle\sigma_{12}\,v\rangle}{\langle\sigma_{13}\,v\rangle} \simeq \frac{g_2}{g_3} = \frac{2J_2+1}{2J_3+1} = \frac{3}{2}\ .$$

This ignores $3\to 2$ transitions and assumes that the doublet states are uncoupled from all other states. This is approximately true. Note that the ratio of the collisional transition rates here is (almost) exactly equal to the ratio of statistical weights due to the very small energy difference between the doublet D-states.

In the *high density limit* ($N_e \geq 2\times 10^4\,\mathrm{cm}^{-3}$),

$$r = \frac{j(\lambda 3729)}{j(\lambda 3726)} = \frac{N_1 A_{21}\langle\sigma_{12}\,v\rangle\,\langle\sigma_{31}\,v\rangle\,h\nu_{21}}{N_1 A_{31}\langle\sigma_{21}\,v\rangle\,\langle\sigma_{13}\,v\rangle\,h\nu_{31}} = \frac{A_{21}\,g_2}{A_{31}\,g_3} = 0.3\ .$$

Again, we have ignored the very small energy difference $E_3 - E_2$ in expressing the ratio of collision rates.

In between the limits, one transition is *above* its critical density and the other is *below*. It is easy to verify that

$$r = \frac{j(\lambda 3729)}{j(\lambda 3726)} = \frac{A_{21}\,g_2}{N_e\langle\sigma_{21}\,v\rangle\,g_3} \propto \frac{1}{N_e}\ .$$

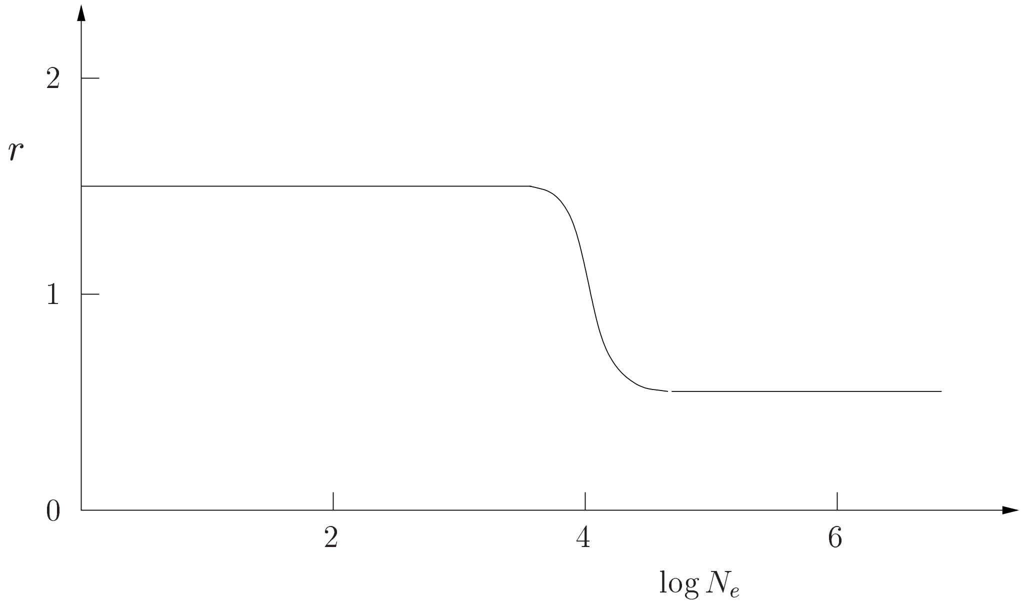

Clearly, it is a simple matter to determine N_e from the observation of the line ratio r *if* the density is in the range $4\times 10^3 - 2\times 10^4\,\mathrm{cm}^{-3}$. Otherwise, only limits can be obtained. If the nebula happens to be inhomogeneous in density, then it can be very difficult to interpret the observations of r.

A CASE STUDY

An interesting example, highly relevant to today's techniques for IR and sub-millimeter observations, is the use of *fine structure transitions* in atomic lines of C, N, and O to probe the physical conditions in molecular clouds which are invisible in the optical due to obscuration by dust.

Some relevant data from Table 1 of Watson (*Physica Scripta*, **T11**, 33, 1985) are shown in the following abridged form:

SOME ATOMIC LINE DATA OF ASTROPHYSICAL INTEREST

Transition	Species	ν (GHz)	λ (μm)	A (s^{-1})	N_c (cm^{-3})
${}^2P_{3/2} \to {}^2P_{1/2}$	C II	1900.536	157.8	2.36×10^{-6}	3.0×10^3
${}^3P_2 \to {}^3P_1$	C I	809.343	370.7	2.68×10^{-7}	7.1×10^2
${}^3P_1 \to {}^3P_0$	C I	492.161	609.6	7.93×10^{-8}	1.7×10^2
${}^3P_0 \to {}^3P_1$	O I	2060.061	145.6	1.70×10^{-5}	1.5×10^5
${}^3P_1 \to {}^3P_2$	O I	4744.753	63.2	8.95×10^{-5}	9.8×10^5

Note that the O I triplet is *inverted* because the p-shell is *more* than half full! The ground configuration is $1s^2 2s^2 2p^4$. Except for this difference, it has the same energy-level diagram as O III because their configurations are complementary (see §7.1). Moreover, the C I case is identical to the O III one, having exactly the same electron configuration. In both the C I and O I cases, the triplet P-states lie lowest according to Hund's Rule – one triplet is inverted, the other is not.

Most of these sub-mm transitions can be observed only from space or from high-flying aircraft due to the high opacity of the Earth's atmosphere at these wavelengths. But some can be seen at high redshift from ultra-luminous IR galaxies which are believed to be exceedingly rich in dust and gas and in the early phases of star formation.

Consider the IRAS source F10214+4724 studied by Brown & Vanden Bout (*Ap.J.*, **397**, L11, 1992). From this galaxy, one can detect C I in two transitions. It is believed that the neutral carbon is produced by photo-dissociation of CO in dense *molecular gas* exposed to a source of UV radiation.

- The protogalaxy is at $z = 2.286$ and has nearly all of its luminosity in the IR between $10^{12.5} - 10^{14}$ Hz (from which one can infer $\sim 5 \times 10^9$ $M_\odot$ of dust heated by starburst activity).
- The levels in these atoms are populated by collisions with H_2 molecules and, therefore, provide a probe of the H_2 content and *not* the electron density because $T_{\rm kin} < 2000\,°K$. The temperatures required are only a few hundred Kelvin since the levels are very close to the ground state.
- The figure on the next page shows the results of performing statistical equilibrium calculations on a 3-level system of C I for $T = 200\,°K$, $500\,°K$, and $1000\,°K$.
- The observed ratio $I(2-1)/I(1-0)$ equals 5 which (from the first graph) implies a hydrogen density $N_{\rm H}$ somewhere between $650\,{\rm cm}^{-3}$ and $2500\,{\rm cm}^{-3}$; this range is typical of molecular cloud densities.

Note that in the figure on the next page (I've lost the reference!) the line ratios have been chosen in such a way that r always *increases* with N, unlike my choice in the figure on page **??**. I could have made my sketch look like their plots by simply inverting my definition of r. Also, it's clear that a different notation for line intensities is being employed: instead of $j(\lambda xxxx)$ for intensity, ^{I}[C(n-m)] or ^{I}[O(n-m)] is used instead – no big deal.

ATOMIC LINE RATIOS INVOLVING CARBON AND OXYGEN

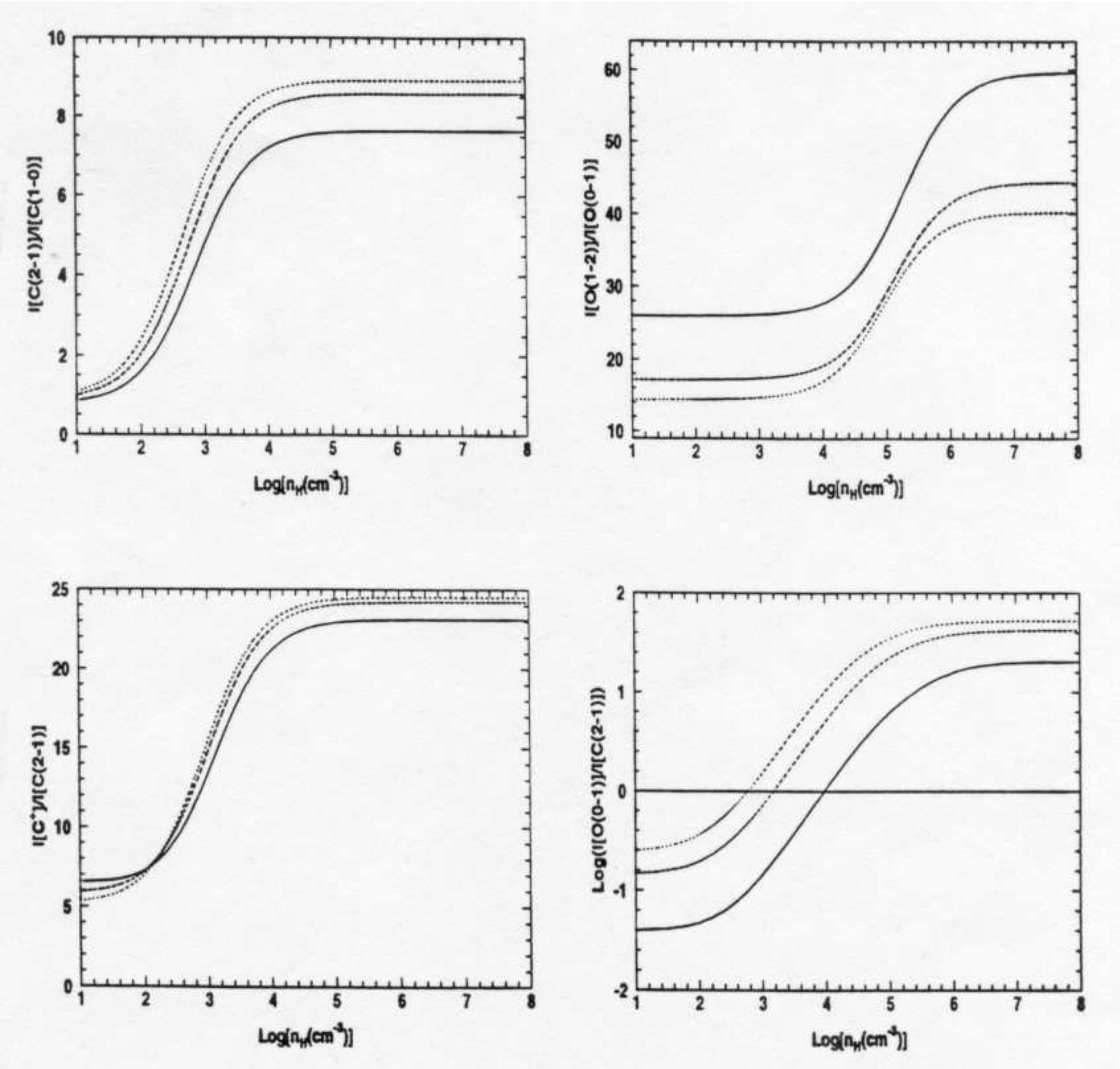

Figure 8.13 – The line ratios of the atomic lines as a function of density and for C/O = 0.5 and $C^+/C^0 = 1$. The solid line is for a gas temperature of $T = 200\,^\circ$K, the dashed line for $T = 500\,^\circ$K, and the dotted line for $T = 1000\,^\circ$K.

8.2 Emission by Interstellar Molecules

There are over 100 different molecules observed in sub-mm, mm, and cm wavelength regions of the spectrum. The most prominent of these (e.g., CO, HCO^+, HCN) are *optically thick* at the lowest transitions of the most abundant isotopes. This makes the analysis of molecular line data very difficult as we shall see. However, the line intensities tend to be relatively *strong* because the collisionally excited transitions are *permitted* ones. Consequently, even very small molecular densities can be detected by modern instruments.

In general, however, we use the fact that the area under the line is proportional to the column density of the relevant molecule by a factor which we can calculate from a model of the source cloud. Note that there may be many (optically thick) clouds along the line of sight but in many cases we can separate their contributions because their radial velocities are all different from one another. This is analogous to 21 cm data (HI) in which we can see the contributions of different spiral arms along the line of sight, shifted with respect to one another.

The main point is that by combining the observations of at least two transitions of a particular molecule we can extract the density not only of the molecule itself but also the density of H_2 which is responsible for the collisional excitations. For this to work, however, there must be a velocity gradient across the source so that the optical depth will be sufficiently small at the line frequency; otherwise, the observer would not be able to "probe" the cloud.

Another aspect of this problem which makes it particularly difficult is that because the molecular line transitions are of such low energy we have to include all the relevant radiative and collisional processes that are responsible for populating the important molecular states. This, together with the optically thick radiative transfer, makes the molecular line problem much more difficult than the analogous atomic line problem that we considered in the last section.

In what follows, I intend to outline only the basic ideas and not worry too much about the details. This is an *advanced* topic!

Basic Modeling Steps

The primary goal is to construct a cloud model which reproduces the observed brightness temperature as a function of frequency (or radial velocity) for all the detected lines. More specifically, we want to calculate the "radiation temperature", $T_{\mathrm{R}}(\nu)$, where

$$T_{\mathrm{R}}(\nu) \equiv \frac{c^2}{2k\nu^2}\,(I_\nu - I_{2.7})$$

which differs from the brightness temperature T_b in that we allow for 2.7 °K blackbody background which is significant in this context because these molecules exist only in *cool* clouds ($T \sim 10-20$ °K).

This is a *coupled* radiative transfer and statistical equilibrium problem. There are *three* basic steps:

(1) Specify the basic physical parameters: $n(H_2)$, molecular abundance relative to H_2, the kinetic temperature T_{kin}, cloud kinematics in the form of a velocity gradient across the cloud.

(2) Make an initial guess for the integrated line intensity $\bar{J}_{\mathrm{L}}$. Determine the excitation temperatures (i.e., population numbers) of all the levels of interest and from these the optical depths τ_ν of all the lines.

(3) Evaluate I_ν and, thereby, $T_{\rm R}(\nu)$ for all the lines. Iterate $\bar{J}_\nu$ to convergence. Compare with observation and adjust the input parameters until one can fit all the lines simultaneously.

Statistical Equilibrium

Assume steady state and that the molecular system we are dealing with has N levels which are involved in the populating and depopulating of the states responsible for the observed lines. For the $i^{\rm th}$ level, statistical equilibrium can be expressed schematically as

$$\underbrace{\sum_{j=1}^{N} n_j\, k_{ji}}_{\text{population rate}} \quad = \quad \underbrace{n_i \sum_{j=1}^{N} k_{ij}}_{\text{depopulation rate}} \qquad (j \neq i)$$

where $n_j \equiv$ population number (per unit volume) of the $j^{\rm th}$ state. Also, the k_{ij} and k_{ji} are the "rate coefficients" which incorporate spontaneous transitions, absorptions, stimulated emissions, and collisions (with H_2):

$$k_{ij} = A_{ij} + B_{ij}\,\bar{J}_{ij} + C_{ij}$$

where $A_{ij} = 0$ if $i < j$. Also, $\bar{J}_{ij}$ is the intensity averaged over the line ($= \bar{J}_\nu$).

In the end, we have a set of $N-1$ inhomogeneous equations which can, in principle, be solved because we have assumed values for $T_{\rm kin}$, $n({\rm H_2})$, $n(\text{molecule})/n({\rm H_2})$ (a constraint which reduces the N unknowns to $N-1$), and we can estimate $\bar{J}_{ij}$ by a scheme outlined in the next section. We actually end up with all the population numbers relative to $n({\rm H_2})$.

Just like the atomic line problem that we considered earlier, there are two limiting density regimes:

(a) Complete thermalization (high density)

The collision rate $C_{u\ell}$ ($\equiv n({\rm H_2})\, R_{u\ell}$, say) from the upper to the lower state *exceeds* the corresponding radiative rate $A_{u\ell}$:

$$C_{u\ell} > A_{u\ell} \quad \Longrightarrow \quad n({\rm H_2}) > n_{\rm crit} \equiv \frac{A_{u\ell}}{R_{u\ell}} \quad \Longrightarrow \quad T_{\rm ex} = T_{\rm kin} \quad \text{(thermalized)}.$$

(b) Low collision rate (low density)

$$n({\rm H_2}) < n_{\rm crit} \quad \Longrightarrow \quad T_{\rm ex} < T_{\rm kin} \quad \text{(non-thermal)}.$$

In this low-density regime, emission depends more strongly on the density as we saw earlier.

Here are some sample values of the critical density for a number of molecular transitions:

VALUES OF $n_{\rm crit}$ FOR SOME ROTATIONAL TRANSITIONS

Molecule	Transition	ν (GHz)	$n_{\rm crit}$ (cm^{-3})
CO	$J = 1-0$	115	2×10^3
	$J = 2-1$	230	1×10^4
	$J = 3-2$	345	4×10^4
CS	$J = 5-4$	245	7×10^6
	$J = 7-6$	343	2×10^7
HCN	$J = 4-3$	355	2×10^8
HCO^+	$J = 4-3$	357	2×10^7

Molecular hydrogen densities can be as high as $10^4\,\mathrm{cm}^{-3}$ in some clouds, in which case, CO lines could be thermalized. But the lines of other molecules would normally not be.

The Large Velocity Gradient Method (LVG)

References:

- Castor (1970), *MNRAS*, **149**, 111
- Goldreich & Kwan (1974), *ApJ*, **189**, 441
- DeJong et al. (1975), *ApJ*, **199**, 69
- Rybicki & Hummer (1978), *ApJ*, **219**, 654

This is an approximate technique for simplifying the radiative transfer problem sufficiently to yield an expression for $\bar{J}_\nu$ which is needed (as we just saw) to solve the statistical equilibrium problem.

In the general case, one must solve the coupled radiative transfer and statistical equilibrium problems together (i.e., simultaneously). This is due to the dependence on $\bar{J}_\nu$ which can be determined only by evaluating I_ν as integrals over the source function along optical paths in all directions.

However, considerable simplification occurs *if* a large velocity gradient exists across the cloud. In that case, if the Doppler width of a line (ΔV_D, say) is much less than the velocity difference (ΔV) across the cloud, then a photon emitted at a point P can be absorbed only within a short distance ℓ from P; i.e.,

$$\ell \simeq R\,\frac{\Delta V_\mathrm{D}}{\Delta V} = \Delta V_\mathrm{D}\left(\frac{dv}{ds}\right)^{-1} \ll R$$

where R is the cloud scale or dimension. This is called the "Sobolev approximation" which applies wherever the effective optical depth ($\ell\kappa$) is much smaller that the optical depth of the whole cloud in the absence of a velocity gradient.

Let's consider the basics of radiative transfer in a moving medium – one with a velocity gradient. This is a generic problem in astrophysics (e.g., stellar winds, mass inflows and outflows from galactic nuclei and star-forming regions). We want to focus on the analytics rather than the numerics. Recall that

$$d\tau_\nu = \alpha_\nu\,ds = \frac{h\nu_{u\ell}}{4\pi}\,\phi(\nu)\,(n_\ell B_{\ell u} - n_u B_{u\ell})\,ds$$

where ds is the element of path length. The total optical depth may then be written as

$$\tau_\nu = \frac{h\nu_{u\ell}}{4\pi}\,(n_\ell B_{\ell u} - n_u B_{u\ell})\int_0^\infty \phi(\nu_s)\,ds$$

where ν_s is the Doppler shift value of ν at position s in the cloud. That is, $\phi(\nu_s)$ depends on s when there is a velocity gradient; that is why it is under the integral sign. A velocity gradient introduces a velocity shift or a frequency shift with distance and, therefore, different parts of the absorption profile $\phi(\nu)$ will be sampled at different s.

Thus, if $\phi(\nu)$ is the line profile where the intensity is being measured (the observer's position, say, at $s = 0$), then the profile at some distant point s is $\phi(\nu_s) \equiv \phi(\nu - \nu')$ where

$$\nu' = \frac{\nu_{u\ell}}{c}\,v = \frac{\nu_{u\ell}}{c}\left(\frac{dv}{ds}\right)s \qquad \Longrightarrow \qquad ds = \frac{c}{\nu_{u\ell}}\left(\frac{dv}{ds}\right)^{-1} d\nu'.$$

Then the optical depth through the cloud can be written as

$$\tau_\nu = \tau \int_{\nu'_n}^{\nu'_m} \phi(\nu - \nu')\, d\nu' = \tau w_\nu \quad \text{(say)}$$

where ν'_n and ν'_m delineate the Doppler shift range; they correspond respectively to the minimum and maximum velocities in the cloud, normally the near-side and far-side values or vice-versa if the velocities are negative (blue shifts). Also, τ is the optical depth at the line center and w_ν is the fraction of the Doppler-shifted absorption profile which falls within the velocity range of the cloud:

$$\tau \equiv \frac{h\nu_{u\ell}}{4\pi}\,(n_\ell B_{\ell u} - n_u B_{u\ell})\left(\frac{dv}{ds}\right)^{-1}\frac{c}{\nu_{u\ell}} \qquad \text{and} \qquad w_\nu = \int_{\nu-\nu'_m}^{\nu-\nu'_n} \phi(x)\, dx \ .$$

Clearly, $\tau_\nu \to \tau$ when the absorption profile bandwidth, $\nu_o \pm \Delta\nu_{\rm D}$, falls entirely within the Doppler range. When the absorption profile overlaps either boundary of the Doppler range, τ_ν will lie somewhere between 0 and τ. And, finally, the observer sees nothing if the Doppler range fails to overlap any of the absorption bandwidth.

Note that this over-simplified analysis makes no allowance for density variations within the cloud. In reality, molecular clouds are close to virial equilibrium and, therefore, are centrally concentrated. Hence, τ_ν should rise and fall as the observer scans through the cloud center. He should observe a normal Doppler-broadened line and does (see the example at the end of this section). But at least this analysis demonstrates clearly that it is the nonzero velocity gradient that reduces what would be an infinite τ to a *finite* one. This is the whole point of this exercise.

The formal solution to the equation of transfer now gives us an expression for I_ν at the observer's position or, in fact, at any arbitrary point including *within* the cloud (in which case, τ would be the optical depth to the boundary in the (reverse) direction of I_ν):

$$I_\nu = I_{\rm L}\,\phi(\nu) \quad \text{where} \quad I_{\rm L} = S_{\rm L}\left(1 - {\rm e}^{-\tau w_\nu}\right) + I_{\rm B}\,{\rm e}^{-\tau w_\nu}$$

where $S_{\rm L} = S_{u\ell} = S_{\nu_o}$ is the source function (integrated over the line) and $I_{\rm B}$ is the background blackbody intensity (again integrated over the line).

In the statistical equilibrium calculation, we need at some arbitrary point in the cloud the mean intensity in the line; we ignore boundary effects and assume that I_ν is *isotropic*:

$$\bar{J}_{\rm L} = \int_0^\infty I_{\rm L}\,\phi(\nu)\, d\nu = S_{\rm L}\int_0^\infty \phi(\nu)\left(1 - {\rm e}^{-\tau w_\nu}\right) d\nu + I_{\rm B}\int_0^\infty \phi(\nu)\,{\rm e}^{-\tau w_\nu}\, d\nu$$

which after a change in variable from ν to w_ν becomes

$$\bar{J}_{\rm L} = S_{\rm L}\int_0^1 \left(1 - {\rm e}^{-\tau w_\nu}\right) dw_\nu + I_{\rm B}\int_0^1 {\rm e}^{-\tau w_\nu}\, dw_\nu = (1-\beta)S_{\rm L} + \beta I_{\rm B}$$

where

$$\beta \equiv \frac{(1 - {\rm e}^{-\tau})}{\tau} \longrightarrow \begin{cases} 0 & \text{as } \ \tau \to \infty \ , \\ 1 - \frac{\tau}{2} & \text{as } \ \tau \to 0 \ . \end{cases}$$

In the calculation of $\bar{J}_{\rm L}$, we are integrating from the observer's position through the cloud but it is possible to apply the expression for the line intensity at some arbitrary point *within* the cloud IF we adjust τ accordingly. Thus, for example, we might replace τ by $\tau/2$ to get $\bar{J}_{\rm L}$ at the center of the cloud because this would be the typical depth to the boundary along any (reverse) direction of

I_ν. Note that in the above expression for β, we have shown that the mean optical depth averaged over the line is also $\tau/2$ in the limit of small τ.

The limits on the frequency (0 to ∞) are still the same due to the assumption of large Doppler shifts across the cloud. Our dv/ds is *some average* over position and direction. In the final analysis, we can't really determine dv/ds but only

$$\frac{n(\text{molecule})}{n(\text{H}_2)} \left(\frac{dv}{ds}\right)^{-1}_{\text{mean}}$$

as a look at the definition of τ will reveal. The bottom line is that $\bar{J}_\text{L}$ is determined by a *local* optical depth within the cloud.

Modeling Procedure

(a) Choose T_kin, $n(\text{H}_2)$, and
$$x \equiv \frac{n(\text{molecule})}{n(\text{H}_2)} \left(\frac{dv}{ds}\right)^{-1}_{\text{mean}} .$$

(b) Adopt an initial guess for the mean line intensity $\bar{J}_\text{L}$. With this, we can compute the population numbers n_i (equivalent to excitation temperatures $T_{\text{ex},i}$) which in turn can be used to find τ and S_L. These provide a new estimate of the line intensity.

(c) Repeat by solving the statistical equilibrium equations for the new values of $T_{\text{ex},i}$ and iterate until the $T_{\text{ex},i}$ (or n_i) converge. Include, of course, the effects of the background I_B.

(d) Finally, compute I_ν and the predicted radiation temperatures $T_\text{R}(\nu)$ for all the observed lines.

(e) Repeat for a range of $n(\text{H}_2)$ and x. Then plot contours of *constant* T_R (equal to the observed values) for several transitions in a $\log n(\text{H}_2) - \log x$ diagram. Hopefully, the contours will all cross at a particular $(n(\text{H}_2), x)$ point at which one can read off the model solution or fit.

As an example, consider the CO data analyzed by Richardson et al. (1985, *ApJ*, **290**, 637). In the source DR21, they chose three transitions of CO:

$$\begin{aligned} J &= 1-0 \quad (115\,\text{GHz}), \\ J &= 2-1 \quad (230\,\text{GHz}), \\ J &= 3-2 \quad (345\,\text{GHz}) \end{aligned}$$

and concentrated on frequencies in the line wings, corresponding to the *outflow regions*.

Notice that in the $\log n(\text{H}_2) - \log x$ diagram on page **??** there is also a contour of constant ratio

$$r_{31} \equiv \frac{T_\text{R}(3-2)}{T_\text{R}(1-0)} = 1.1$$

which is a check for calibration errors. At low x, the contour approaches a constant value of $n(\text{H}_2)$ because in this limit the gas is optically thin and the ratio r_{31} is determined entirely by the collision rates to the excited levels.

As you can see in the diagram (Fig. 8.22), the model fit is "perfect"; all 4 contours cross at the same point and yield

$$\log n(\text{H}_2) = 4.0 \quad \text{and} \quad \log x = -6.7 .$$

To convert x into $n(\mathrm{CO})$ is, of course, difficult because we don't really know what dv/ds is. But a rough guess can be made by assuming that v is *linear* in s in which case

$$\frac{dv}{ds} \sim \frac{\Delta V}{R} = \frac{\text{velocity half-width of line}}{\text{scale of outflow region}} \simeq \frac{10\,\mathrm{km\,s^{-1}}}{1\,\mathrm{pc}} \ .$$

Keep in mind, however, that some sources are apparently better fit with a v that is *nonlinear* in s. We now have

$$\frac{n(\mathrm{CO})}{n(\mathrm{H_2})} \simeq 10^{-6.7}\,\frac{\Delta V}{R} \simeq \frac{10^{-6.7} \times 10}{1} = 2 \times 10^{-6} \ .$$

The authors argue that in many outflow regions, x_{out} is much smaller than that estimated (x_{est}) from studies of quiescent molecular gas with no velocity gradient – perhaps by a factor larger than 10! Is this due to smaller $n(\mathrm{CO})$ or larger dv/ds? Probably the latter is my guess.

The foregoing abundance ratio is my own calculation. Richardson et al. had no interest in the molecular abundance of CO which is only a trace element after all. The physically important quantities are $n(\mathrm{H_2})$ and (perhaps) dv/ds. The actual abundance of CO derived from the above ratio and the computed abundance of $\mathrm{H_2}$ is quite small:

$$n(\mathrm{CO}) \sim 2 \times 10^{-2}\,\mathrm{cm^{-3}} \ .$$

This corresponds to a column density through the 1 pc region of

$$2 \times 10^{-2}\,\mathrm{cm^{-3}} \times 3 \times 10^{18}\,\mathrm{cm} \sim 6 \times 10^{16}\,\mathrm{cm^{-2}} \ .$$

CO Line Profile for the IRAS Source DR21

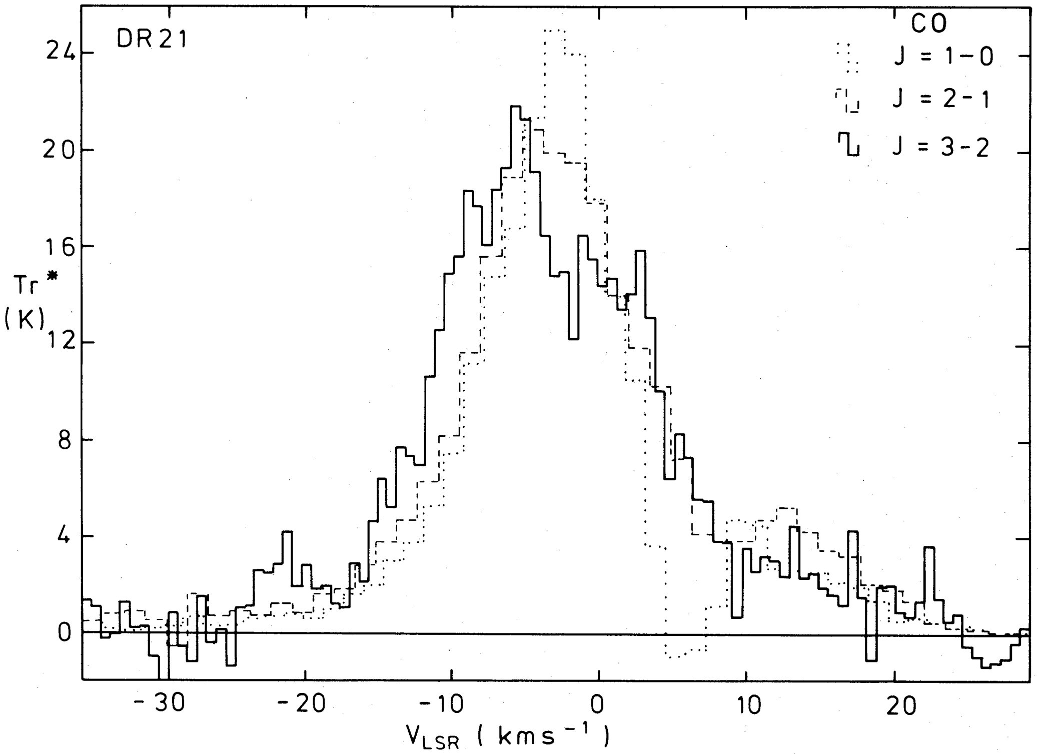

Figure 8.21 – The CO $J = 3-2$ spectrum of DR21, superposed on the $J = 2-1$ and the $J = 1-0$ spectra of Plambeck, Snell, and Loren (1983, *ApJ*, **266**, 321).

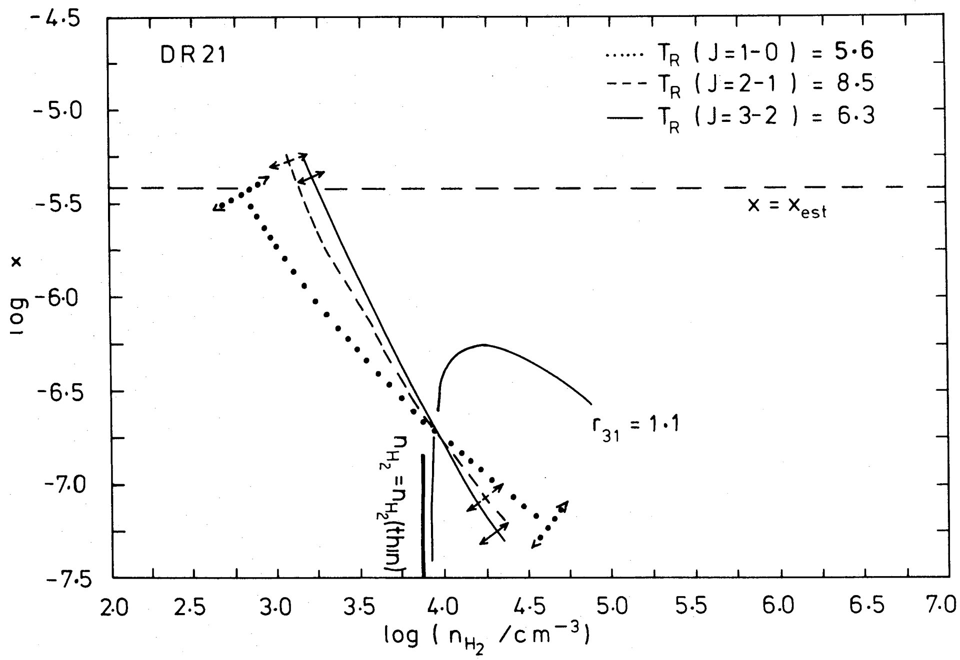

Figure 8.22 – Contours of $T_{\rm R}$ for the $J = 1-0$, $J = 2-1$, and $J = 3-2$ transitions of CO in DR21 based on the LVG model described in §8.2. Arrows show the effect of ±30% errors in the observations of each line. Also shown are the lines of $x = x_{\rm est}$ and $n_{\rm H_2} = n_{\rm H_2}$(thin) and the line of constant r_{31} appropriate to the observations of this source.

8.3 Interstellar Absorption Lines

The first interstellar absorption lines were discovered in 1904. They were the H and K lines of Ca II observed in the spectra of O and B stars just where you wouldn't expect to see such lines because they are normally associated with cool stars. Also, interstellar lines were observed in the spectra of cool, binary stars where it was noticed that some lines remained *fixed* in wavelength and didn't participate in the normal Doppler swings. Later, Struve discovered that the strengths of the H and K lines increase with the distances of the stars but not smoothly. This indicates that the interstellar gas in not uniformly distributed. In 1936, Beals noticed that under high dispersion the lines were almost always *multiple*. Thus, the picture developed of an interstellar medium filled with clouds of gas and dust, the latter causing extinction and reddening. These clouds moved about with random velocities of order $10\,\mathrm{km\,s^{-1}}$.

__Basic Points__

1. **The Degree Of Excitation Is Effectively Zero**

   The first thing to realize about interstellar atoms and ions is that they are almost all in the *ground state*. This is because both collisional and radiative excitation rates are very small (due to low densities, small kinetic energies, and weak radiation fields) but spontaneous de-excitation takes place at a rate which depends only on the Einstein coefficient A_{ji}. Thus, we don't expect to see any Balmer absorption lines. But there should be very strong Lyman lines in the ultraviolet (912 – 1215Å) and, indeed, they are observed by UV satellites. Another obvious consequence of hydrogen atoms being mostly in the ground state is that the ISM is *opaque* to Lyman continuum ($\lambda < 912$Å).

   Absorption lines are observed over the whole electromagnetic spectrum, including the microwave and radio bands. In the optical, the most commonly observed interstellar lines are probably those of Ca and Na, not because these elements are the most abundant but just because their lines happen to fall in the visible part of the spectrum.

2. **The Degree Of Ionization Is NOT Zero**

   Another basic point has to do with the degree of ionization. At first thought, one might think that nothing would be ionized but this is not the case. We have already considered Ca II for example. It *is* true that the rates of photoionization and collisional ionization are very low due to the low radiation intensities and the low particle densities. But, on the other hand, the rate of recombination is also very low. A Ca II ion, for example, will fly around for *months* typically before it finds an electron! Therefore, both ions and neutral atoms can co-exist in deep space. The only safe thing that one can say is that both atoms and ions will be in their ground states. The actual degree of ionization will be determined by the equations of statistical equilibrium; i.e., by the relative rates of photoionization (by starlight, X-rays, etc.), collisional ionization (including that of cosmic rays), and recombination (which depends, of course, on N_e and T_e). This is the problem of "ionization equilibrium" which is discussed briefly at the end of this section.

Curve of Growth Analysis for Interstellar Lines

At the absorption line frequency, the optical depth between the observer and the background star is nonzero. If I^*_ν is the specific intensity at the surface of the star, then the observer sees

$$F_\nu = \oint I^*_\nu \, \mathrm{e}^{-\tau_\nu} \cos\theta \, d\omega \simeq I^*_\nu \, \mathrm{e}^{-\tau_\nu} \, \Delta\omega$$

where the solid angle subtended by the star is $\Delta\omega = \pi R^2/r^2$. In the continuum, the optical depth is relatively small (assume *zero*) in which case $F_c = I^*_c \Delta\omega = I^*_\nu \Delta\omega$ if there is no absorption line in the stellar atmosphere at that frequency. Therefore,

$$W_\lambda = \int_0^\infty \left(1 - \frac{F_\nu}{F_c}\right) d\lambda = \int_0^\infty \left(1 - \mathrm{e}^{-\tau_\lambda}\right) d\lambda \ .$$

Now look at the expression for τ_λ; it is the integral of the absorption coefficient per unit volume along the line-of-sight to the star:

$$\tau_\lambda \equiv \int \rho \ell_\lambda \, ds = \int N a_\lambda \, ds = a_\lambda \, \tilde{N}$$

where $\tilde{N}$ is the column density (or the number of absorbing atoms per unit area) between the observer and the star. Let's adopt the Voigt absorption profile; it is commonly used to describe the broadening effects of Doppler motions and particle collisions in stellar atmospheres. Thus,

$$a_\lambda = \frac{\rho \ell_\lambda}{N} = \frac{\pi e^2}{mc} f \, \frac{U(b,v)}{\Delta\nu_{\mathrm{D}}} = a_o \sqrt{\pi} \, U(b,v)$$

where a_o is the absorption coefficient per atom at the line center; that is

$$a_o \equiv \frac{\pi e^2}{mc} \frac{f}{\sqrt{\pi}} \frac{\lambda}{\xi_o} \quad \text{since} \quad \Delta\nu_{\mathrm{D}} \equiv \frac{\xi_o}{c} \nu = \frac{\xi_o}{\lambda} \ .$$

The Voigt profile is normalized in the sense that the integral of U over all frequency is unity. The function has two arguments: the first one, b, is really a *parameter* – it is the ratio of the collisional and Doppler widths. The second one, v, is a dimensionless frequency: $v \equiv (\nu - \nu_o)/\Delta\nu_{\mathrm{D}}$ – actually a measure of the displacement from line center.

In the interstellar medium, collisional broadening is unimportant as you might expect. Also, absorption lines are generally very weak. Both of these circumstances mean that the line wings are not very well developed (i.e., $b \simeq 0$). Thus, we are left with only the Doppler core:

$$U(b,v) \simeq \frac{\mathrm{e}^{-v^2}}{\sqrt{\pi}} \qquad \Longrightarrow \qquad a_\lambda = a_o \, \mathrm{e}^{-v^2} \ .$$

Therefore,

$$\tau_\lambda = \tilde{N} \, a_\lambda = \tilde{N} \, a_o \, \mathrm{e}^{-v^2} = \tau_o \, \mathrm{e}^{-v^2} \quad \text{(say)}$$

where τ_o is the optical depth at the line center. In addition, we have

$$d\lambda = -\frac{\lambda^2}{c} \, d\nu = -\frac{\lambda^2}{c} \, \Delta\nu_{\mathrm{D}} \, dv = -\frac{\lambda^2}{c} \frac{\xi_o}{\lambda} \, dv = -\frac{\lambda \xi_o}{c} \, dv \ .$$

With this substitution, the equivalent width becomes

$$\frac{W_\lambda}{\lambda} \frac{c}{\xi_o} = \int_{-\infty}^{\infty} \left[1 - \exp\left(-\tau_o \, \mathrm{e}^{-v^2}\right)\right] dv \ ,$$

which is some function of τ_o. There is an obvious problem here: a measurement of W_λ gives τ_o (and, of course, $\tilde{N}$) only if ξ_o is known. Very weak lines are an exception, however, because ξ_o drops out. To see this, let $\tau_o \ll 1$ which implies

$$\frac{W_\lambda}{\lambda}\frac{c}{\xi_o} = \int_{-\infty}^{\infty}\left(\tau_o\,\mathrm{e}^{-v^2} + \ldots\right) dv = \tau_o\sqrt{\pi} = \tilde{N}\,a_o\,\sqrt{\pi} = \tilde{N}\,\frac{\pi e^2}{mc}\,\frac{\lambda}{\xi_o}\,f\ .$$

Thus,

$$W_\lambda = \lambda^2\,\frac{\sqrt{\pi}e^2}{mc^2}\,\tilde{N}f \qquad \text{(weak lines)}.$$

In this case, knowing the oscillator strength f, we can find $\tilde{N}$ directly from a measurement of W_λ. Clearly for weak lines, Doppler broadening does not affect the equivalent width. The line is broader but shallower and the number of absorptions is unaffected. This is a well-known characteristic of weak stellar absorption lines.

But, for strong or saturated lines, on the other hand, the problem is more difficult because $\tilde{N}$ depends on *both* W_λ and ξ_o. That is, Doppler broadening can increase the equivalent width by pushing atoms in the core where they can't absorb up or down in frequency to where they can. The solution to this dilemma is to appeal to ...

The Doublet Ratio Method

The idea here is to eliminate ξ_o by forming the *ratio* of equivalent widths of two lines of the *same* ion (i.e., with the same $\tilde{N}$). This so-called "doublet ratio" will then depend only on the optical depth τ_o of one of the lines. As examples, this method can be applied to the Ca II H and K lines (3968Å and 3933Å, resp.) and the Na I D_1 and D_2 lines (5895Å and 5889Å, resp.). Also, Na I has a weaker doublet at 3302.34Å and 3302.94Å.

Na I (with 11 electrons) and Ca II (with 19 electrons) each have only *one* electron outside closed shells, so they have the same term structure or energy level diagram as shown below.

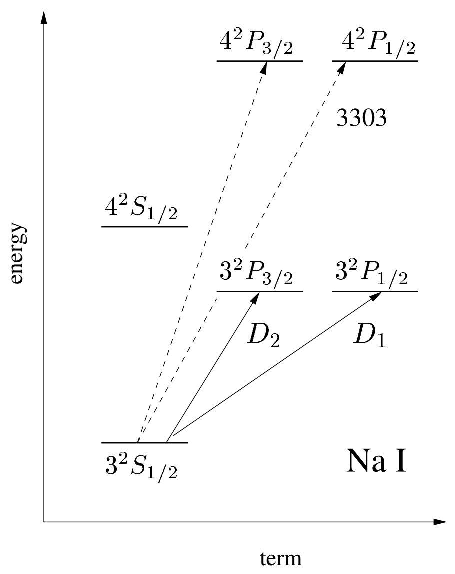

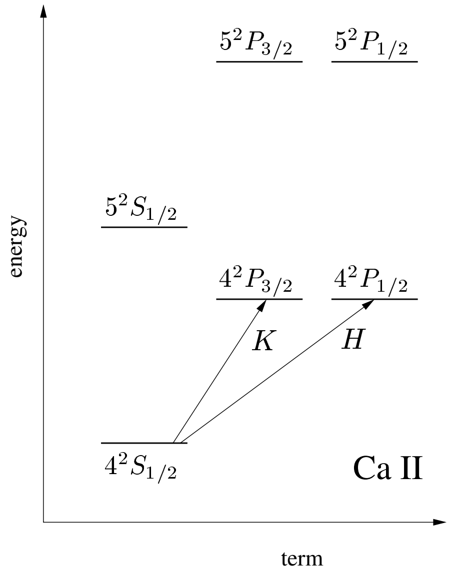

The optical depth in the K line is just *double* that in the H line because the statistical weight of its upper state is twice as large:

$$\begin{aligned}\frac{\tau_o(K)}{\tau_o(H)} &= \frac{\tilde{N}a_o(K)}{\tilde{N}a_o(H)} = \frac{f(K))}{f(H)}\frac{\Delta\nu_{\mathrm{D}}(H)}{\Delta\nu_{\mathrm{D}}(K)} = \frac{f(K))}{f(H)}\frac{\lambda_{\mathrm{K}}}{\lambda_{\mathrm{H}}} \\ &\simeq \frac{f(K))}{f(H)} = \frac{g_{\mathrm{K}}}{g_{\mathrm{H}}} = \frac{2J_{\mathrm{K}}+1}{2J_{\mathrm{H}}+1} = \frac{4}{2} = 2\,.\end{aligned}$$

Similarly, $\tau_o(D_2) = 2\tau_o(D_1)$.

For the Ca II doublet, we now have

$$\frac{W_\lambda(K)}{W_\lambda(H)} = \frac{\int\left[1-\exp\left(-2\tau_o(H)\,\mathrm{e}^{-v^2}\right)\right]dv}{\int\left[1-\exp\left(-\tau_o(H)\,\mathrm{e}^{-v^2}\right)\right]dv} = \mathrm{fcn}[\tau_o(H)]\,.$$

In the limit $\tau_o \ll 1$, it is obvious that the doublet ratio tends asymptotically to 2 whereas in the other limit ($\tau_o \gg 1$), the ratio tends to 1. We can make a table of the doublet ratio as a function of $\tau_o(H)$. In practice, we observe the ratio and then, by the following steps, find $\tilde{N}$:

$$\frac{W_\lambda(K)}{W_\lambda(H)} \overset{\text{Table}}{\Longrightarrow} \tau_o(H) \Longrightarrow \frac{W_\lambda(H)}{\lambda_{\mathrm{H}}}\frac{c}{\xi_o} \Longrightarrow \xi_o \Longrightarrow a_o \Longrightarrow \tilde{N} \equiv \frac{\tau_o}{a_o}\,.$$

Exactly the same procedure applies to Na I D_1 and D_2 lines.

Theoretical Curve of Growth for Na I and Ca II

$\log \tau_o(H)$	$\log\left(\frac{W_\lambda}{\lambda}\frac{c}{\xi_o}\right)$	$\frac{W_\lambda(K)}{W_\lambda(H)}$	$\log\frac{\tilde{N}}{W_\lambda}$	$\frac{W_\lambda(D_1)}{W_\lambda(3303)}$
−0.2	−0.04	1.66	13.06	
0.0	0.11	1.53	13.11	
0.2	0.24	1.39	13.18	
0.4	0.34	1.29	13.28	
0.6	0.42	1.21	13.40	81
0.8	0.48	1.16	13.54	59
1.0	0.52	1.13	13.70	42
1.2	0.56	1.11	13.86	29
1.4	0.59	1.10	14.03	20
1.6	0.62	1.08	14.20	14
1.8	0.64	1.07	14.38	10.2
2.0	0.66	1.07	14.56	7.4

Unfortunately, the method has some limitations:

(i) For $\tau_o \ll 1$, the doublet ratio is a constant (equal to 2 for the H and K lines, for example). We can find $\tilde{N}$, of course, but not ξ_o.

(ii) For $\tau_o \gg 1$, small uncertainties in the doublet ratio translate into large uncertainties in $\tilde{N}$ and ξ_o. This problem can sometimes be bypassed by forming *different* doublets (but each line arising from absorption from the same state). For example, $W_\lambda(D_1)/W_\lambda(3303)$ is more sensitive to large $\tilde{N}$ as shown by the last column in the curve of growth table.

EXAMPLE:

From the spectrum of χ^2 Orionis, we measure

$$W_\lambda(D_1) = 0.39\text{Å} \quad \text{and} \quad W_\lambda(3303) = 0.040\text{Å}$$

from which we calculate the doublet ratio $W_\lambda(D_1)/W_\lambda(3303) = 9.8$. From the curve of growth table, we find $\tilde{N} = 9.8 \times 10^{13}\,\text{cm}^{-2}$ and $\xi_o = 4.5\,\text{km}\,\text{s}^{-1}$.

Such a ξ_o could be the mean velocity of the clouds along the line of sight or it could indicate a mean kinetic temperature of $10^4\,^\circ$K. Obviously, there is a problem of interpretation here and one would have to know the details of any particular situation before making any definite conclusions. However, you should realize that ξ_o will reflect not just the small-scale (thermal) motions of the atoms in the absorbing clouds but also any large-scale (turbulent) motions of these same clouds.

Moreover, there is the problem of translating $\tilde{N}$ into N. Once could estimate the distance to the star in question and, in this way, obtain a mean number density $\langle N \rangle$ along the line of sight. Or, if you happen to know that there are only one or two clouds involved and you can estimate their dimensions, then you have an estimate of the cloud densities.

For determining the *relative* abundances of elements in the interstellar gas, $\tilde{N}$ is just as useful as N. However, we still have the problem of finding the *total* abundance of the element to which the ion belongs. For example, we might want to estimate $N(\text{Ca})$ given $N(\text{Ca\,II})$. In practice, we can't observe absorption lines for *all* the ions of a particular element although the advent of satellites has been a big help in this direction. The other obvious approach is to estimate the degree of ionization and then, knowing the abundance of *one* ion of a particular species, we can find the total abundance of that element. Again, this is the problem of "ionization equilibrium" which is not an easy one to solve.

Ionization Equilibrium of Heavy Atoms in the ISM

It is obvious that the mean radiation intensity J_ν is down by a very large factor in the interstellar medium:

$$J_\nu = D_\nu \langle I_\nu \rangle_{\text{atmos}} \simeq D_\nu \, B_\nu(T_\star)$$

where $T_\star$ is some mean stellar effective temperature weighted by luminosity (about 8000 °K) and

$$D_\nu \equiv \text{dilution factor} = \frac{R^2}{4r^2}\, \mathrm{e}^{-\tau_\nu} \quad \text{for a single star.}$$

Compared to thermodynamic equilibrium, the rate of photoionization is down approximately by a factor D_ν. On the other hand, the rate of recombination which is proportional to N_e, the electron density, is also down by roughly the same factor ($\sim 10^{-17}$). Therefore, it is not obvious whether atoms will be ionized or not. It turns out that both neutral atoms and ions co-exist with some elements like Ca being mostly ionized (Ca II) and others like H being mostly neutral (except near hot stars, of course).

To a rough approximation, one can use Saha's equation with the dilution factor (appropriately averaged over frequency) on the right-hand side. Thus,

$$\frac{N_e N_{j+1}}{N_j} \simeq \bar{D} \left(\frac{N_e N_{j+1}}{N_j} \right)_{\text{Saha}} = 2\bar{D}\, \frac{(2\pi m k T_\star)^{3/2}}{h^3} \frac{g_{o,j+1}}{g_{o,j}}\, \mathrm{e}^{-\chi_j / kT_\star} \,.$$

Note that in the interstellar medium only the *ground* states contribute to the partition functions. The foregoing equation is valid only if (i) all recombinations are to the ground level, and (ii) the starlight is the chief ionizing agent. To do the problem properly, one should really calculate explicitly the rate of ionization from the ground state and the rates of recombination to *all* excited levels *and* allow for the facts that $T_e \neq T_\star$ and that D_ν is a function of frequency. Furthermore, in the case of hydrogen ionization outside H II regions, one must allow for the ionizing effects of X-rays and cosmic-rays because they turn out to be the most important factors.

For *heavy* elements, we can get an approximate idea of the degrees of ionization by neglecting X-rays and cosmic-rays. Then, in equilibrium,

$$\begin{aligned} &\text{Rate of ionization from ground state}(N_j, T_\star, D_\nu) \\ = \;&\text{Rate of recombination to all levels}(N_e, N_{j+1}, T_e) \,. \end{aligned}$$

One finds after some analysis that

$$\frac{N_e N_{j+1}}{N_j} = \mathcal{D}(T_e, T_\star) \left(\frac{T_e}{T_\star} \right)^{1/2} \left(\frac{N_e N_{j+1}}{N_j} \right)_{\text{Saha}}$$

where $\mathcal{D}$ is a complicated integral over frequency. Note that this equation is consistent with the temperature dependence of the recombination coefficient given on page 120; namely, $\langle \sigma_n^{(r)} \rangle \propto T_e^{-1/2}$.

For simple applications, one can ignore absorption (in which case $D_\nu = D \simeq 10^{-14}$) and assume that all recombinations are to the ground state. In this case, $\mathcal{D} = D$. The effect of recombinations to excited levels will clearly *lower* the effective D and the ratio N_{j+1}/N_j. Note that the electron density N_e in the above equation will be due mainly to hydrogen.

It is not necessary, however, to ignore the excited states and people have made accurate calculations taking them into account. Study the tables on the next page; they summarize some results for Ca, Na, and K. A relatively high stellar temperature has been used ($T_\star = 15000$ °K) but the numbers do incorporate recombinations to excited levels. Note the effect of the Lyman continuum and the surprising fact that *higher* stages of ionization are favored in H I regions.

IONIZATION EQUILIBRIUM IN INTERSTELLAR SPACE

Element	j	$N_e N_{j+1}/N_j$		
		100 °K	1000 °K	10000 °K
Ca*	0	14	63	320
Ca	0	230	1200	8200
Ca*	1	0.025	0.11	0.51
Ca	1	0.071	0.31	1.5
Na	0	0.68		24
Na	1	0.018		0.39
K*	0	7.5		260
K	1	0.71		13

*No Lyman continuum

IONIZATION RATIOS FOR AN ASSUMED ELECTRON DENSITY

Ratio	H II Regions ($N_e = 100\,\mathrm{cm}^{-3}$)	H I Regions ($N_e = 0.01\,\mathrm{cm}^{-3}$)	
	Near Hot Stars	Clouds	Intercloud
Ca II/Ca I	82	1400	32000
Ca III/Ca II	0.015	2.5	51
K II/K I		750	26000
K III/K II	0.13		
Na II/Na I	0.24		
Na III/Na II	0.0039		
	↑ Lyman continuum	↑ no Lyman continuum	↑

CONCLUSIONS:

(i) Ca II abundance is always *greater* than Ca I abundance.

(ii) The presence of Lyman continuum has the expected effect; namely, it increases the degree of ionization.

(iii) In H II regions, *lower* stages of ionization are favored whereas the opposite is true in H I regions. This is a density effect, of course, which you can also see in the intercloud regions where $x_{\mathrm{H}} \sim 0.1$ and $T \simeq 10^4\,^\circ$K. The higher T_e between clouds lowers the recombination rate.

The big uncertainty associated with calculations like this is the value of the electron density, N_e. Satellite ultraviolet measurements of the absorption lines of ions such as N I, N II, and N III provide values of N_e, Also, as we have seen, measurements of the dispersion and rotation measures of pulsars give good estimates of the electron density in deep space. These studies indicate that hydrogen is approximately 1% ionized on average in H I regions. That's why I used $N_e = 0.01\,\mathrm{cm}^{-3}$ in the above tables. Such a degree of ionization is much higher than one would expect if starlight were the only ionizing agent (remember that the ISM is opaque to Lyman continuum). Hence, the current belief is that cosmic-rays and X-rays must contribute significantly to the ionization of hydrogen in the ISM. Note that the heavy elements alone contribute very little to the total electron density because one would expect an N_e of only about $10^{-4}\,\mathrm{cm}^{-3}$ if they were the only source of electrons.

A very serious uncertainty at the present time is the relative importance of starlight, cosmic-rays, and X-rays as ionizing agents. Because of this, it is virtually impossible to calculate the degrees of ionization in any accurate way. We really have to rely on observations of interstellar lines from as many degrees of ionization as possible for a given element in order to determine the total abundance of that species. With the help of satellites, this is now being done and a surprising picture has emerged. It appears that the abundances of many heavy elements *in the gas phase* are *under* abundant relative to hydrogen (see a summary of data on next page). There is no reason to expect the relative abundances in the ISM to be any different from the cosmic abundances that we observe in stars. Therefore, it appears inescapable that the missing elements are locked up in dust grains. Whether this occurs by accretion in cool clouds or by condensation in cool stellar atmospheres is not yet known for sure. Probably both mechanisms are at work. In any case, note that the most under-abundant elements (Ca, Ti, Al, Fe, Mn, etc.) have the *highest* condensation temperatures as shown in Field's Fig. 1. They probably form the "seed" nuclei for interstellar grains.

INTERSTELLAR ABUNDANCES: GAS ONLY

G. B. Field, 1974, *ApJ*, **187**, 453-459

COLUMN DENSITIES IN ζ OPHIUCHI

Element	Species	Column Density Log N (cm^{-2})	References
H........	H I	20.61	1
	H_2	20.61	1
Li........	Li I	9.38	2
Be.......	Be II	< 10.92	3
B........	B II	< 13.15	4
C........	C I	14.50	5
	C II	16.75 ± 0.55	5
	CO	14.66	6
N........	N I	16.35 ± 0.75	5
	N II	16.15 ± 0.85	5
O........	O I	17.25 ± 0.35	5
Na.......	Na I	13.69	3, 7
Mg.......	Mg I	12.75 ± 0.45	5
	Mg II	15.40	5
Al........	Al I	< 10.78	8, 9
Si........	Si II	16.15 ± 0.65	5
P........	P II	13.45	5
S.........	S I	13.20	5
	S II	16.15 ± 0.65	5
Ar.......	Ar I	15.05 ± 0.65	5
K........	K I	11.81	10
Ca.......	Ca I	9.67	11, 12
	Ca II	11.73	3, 13
Ti........	Ti I	< 11.04	3
	Ti II	< 11.20	3
Mn.......	Mn II	13.30 ± 0.10	5
Fe.......	Fe I	11.55	8, 9
	Fe II	15.20 ± 0.80	5

REFERENCES.—(1) Spitzer *et al.* 1973; (2) Traub and Carleton 1973; (3) Herbig 1968; (4) Smith and Stecher 1971; (5) Morton *et al.* 1973; (6) Jenkins *et al.* 1973; (7) Hobbs 1969; (8) Bortolot 1972; (9) Shulman 1973; (10) Hobbs 1973; (11) White 1973; (12) Bortolot, Thaddeus, and Shulman 1971; (13) Marschall and Hobbs 1972.

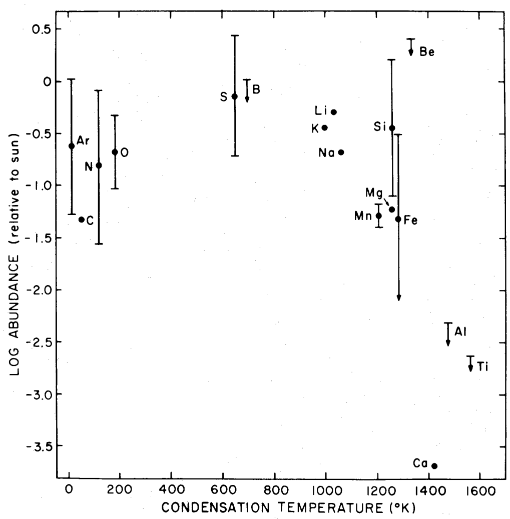

FIG. 1.—Logarithmic abundances of gas-phase elements in ζ Oph, relative to solar-system values, plotted against the condensation temperature calculated for an oxygen-rich atmosphere (table 3). It is suggested that elements above 500° K condensed as cores in stellar nebulae or atmospheres, while those below 500° K condensed as mantles in interstellar space. The large deficiencies of C and Ca are consistent with the latter process.

ABUNDANCES OF THE ELEMENTS

Number (1)	Element (2)	Abundance, ζ_2 Oph log N (cm^{-2}) (3)	Abundance, Solar System log N_s (cm^{-2}) (4)	log (N/N_s) (5)
1...........	H	21.10	21.10*	0.00*
3...........	Li	12.03	12.29	−0.26
4...........	Be	< 10.92	10.51	< 0.41
5...........	B	< 13.15	13.14	< 0.01
6...........	C	16.35	17.67	−1.32
7...........	N	16.35 ± 0.75	17.17	−0.82 ± 0.75
8...........	O	17.25 ± 0.35	17.93	−0.68 ± 0.35
11...........	Na	14.71	15.38	−0.67
12...........	Mg	15.40	16.63	−1.23
13...........	Ai	< 13.32	15.62	< −2.30
14...........	Si	16.15 ± 0.65	16.60	−0.45 ± 0.65
15...........	P	< 13.45	14.58	< −1.13
16...........	S	16.15 ± 0.65	16.30	−0.15 ± 0.65
18...........	Ar	15.05 ± 0.65	15.67	−0.62 ± 0.65
19...........	K	13.77	14.22	−0.45
20...........	Ca	11.77	15.46	−3.69
22...........	Ti	< 11.43	14.04	< −2.61
25...........	Mn	13.30 ± 0.10	14.57	−1.27 ± 0.10
26...........	Fe	< 15.20 ± 0.80	16.52	< −1.32 ± 0.80

* Abundances are normalized so that N_s(H) = N(H).